2026 IEEE/SICE International Symposium on System Integration (SII)
January 11-14, 2026. Cancún, México

Additively Manufactured Inductive Sensor for Translational Motion in Robotic Applications

Robin Waltersbacher
Work-Life Robotics Institute
University of Offenburg
Offenburg, Germany
https://orcid.org/0009-0008-9967-9987

Lukas Stiglmeier
Work-Life Robotics Institute
University of Offenburg
Offenburg, Germany
https://orcid.org/0000-0002-0669-511X

Thomas M. Wendt
Work-Life Robotics Institute
University of Offenburg
Offenburg, Germany
https://orcid.org/0000-0002-4461-5520

***Abstract*—The following contribution presents a fully additively manufactured inductive displacement sensor applied to a model of a translationally movable robot flange. In addition to demonstrating the feasibility of 3D-printed coils, the focus is particularly on their inductive properties and the variation of inductance as a function of translational displacement. For this purpose, two coils are entirely additively manufactured and integrated into the flange of a 3D-printed robot model. Through translational movement of the flange, the overlap between the two opposing coils changes, enabling position detection by measuring the series inductance. The advantage of such additively manufactured approaches lies in their adaptability to diverse application requirements and their capability to realize complex geometries.**

***Index Terms*—3D-Printed Electronics, Additively Manufactured Sensors, Inductive Measurement, Robotics**

I. Introduction

Continuous advancements in additive manufacturing technologies are contributing to the ongoing development of sensor fabrication methods [1], [2]. Examples are additively manufactured torque sensors [3], capacitive displacement sensors [4], and force sensors [5]. Advanced materials such as printable silver ink [6] and carbon nanotubes [7] are also part of current research. The application of additive manufacturing technologies in robotics enables the development of cost-efficient and application-specific solutions that can be precisely tailored to the respective robotic system. For this reason, two fully additively manufactured coil bodies are investigated in this contribution with respect to their functionality as inductive displacement sensors. For the potential use of these coils Fig. 1 shows the inductive displacement sensor integrated into a robot flange, with the coils at 0 mm displacement (a) and at a translational displacement of 50 mm (b). Additive manufacturing offers advantages such as a high degree of customization and material efficiency compared to conventional manufacturing methods [8].

The work in [9] demonstrates a proof of concept for a fully 3D-printed wireless power transfer system and [10] presents an inductive displacement sensor with a 3D-printed sensor body where the body consists of built-in channels into which copper wire is inserted to form the conductive turns of the coils.

Regarding coil displacement, [11], [12] and [13] have shown that a vertical displacement between coils negatively affects their inductive coupling, transmission efficiency and mutual inductance. Optimal performance is achieved when the two coils are fully aligned. The decrease in performance occurs for both positive and negative displacements between the coils and exhibits largely symmetrical behavior in both directions.

Leveraging previous findings, this contribution focuses on a fully 3D-printed sensor system and its behavior under translational coil displacement, which directly affects the inductance measured in series. A key distinction from [10] is that the coils in the present work were entirely manufactured additively.

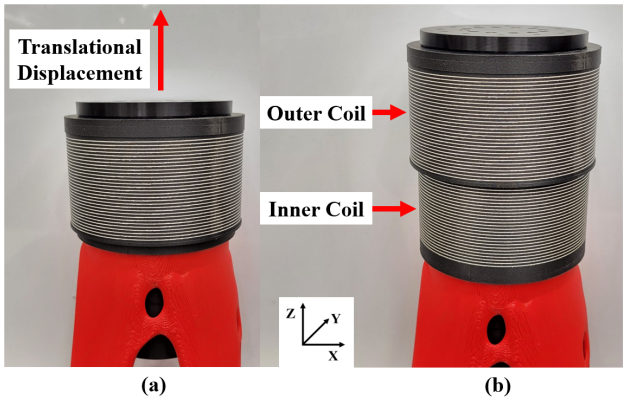

Fig. 1. Inductive displacement sensing for horizontally movable robot flange with 0 mm displacement (a) and 50 mm displacement (b)

II. Fabrication

For the base structure of the coils, PA12 CF15 material from Fiberlogy was used and the conductive traces were fabricated deploying a Neotech AMT 15XSA. This advanced 3D printer is equipped with a 5-axis system, enabling the fabrication of complex geometries. The silver ink LOCTITE ECI 1011 from Henkel was applied utilizing a PICO Pµlse Jetting Valve of Nordson. The coil manufacturing process is described in greater detail in [14], which also investigates their suitability for inductive power transfer applications.

978-1-6654-5784-2/26/$31.00 ©2026 IEEE

III. Analysis and Measurements

A. Analysis and Measurement of the Self Inductance

The two coils are analyzed individually based on their parameters to determine the self-inductance. The inner coil C_I has a coil radius r of 49.5 mm. The outer coil C_O has a coil radius r of 52.5 mm. Both coils have the same length l of 52.5 mm and consist of 30 turns N. Considering the length-to-radius ratio of the two coils, (1) has been identified as the most suitable formula [14]. This formula is a rearranged approximation formula derived by Marce Mathieu in 1934 [15], which closely resembles the widely used approximation for long cylindrical coils where the length is significantly greater than the radius.

$$L = \frac{\mu_0 \cdot \mu_r \cdot N^2 \cdot A}{l + 0.9 \cdot r} \tag{1}$$

By applying the given values of r, l, and N in (1), the calculated self-inductance is 89.71 µH for the inner coil and 98.18 µH for the outer coil.

As the next step, the results from the analytical calculation are validated employing Finite Element Analysis (FEA) software COMSOL Multiphysics. The simulation results are 91.09 µH for the inner coil and 99.7 µH for the outer coil.

The following measurements of the self-inductance and series inductance were conducted utilizing the LCR meter ST2829C from Sourcetronic. For all inductive measurements, a frequency of 100 kHz and a test current of 1 mA were set. For both self-induction and serial induction, 110 measured values were recorded per measurement and the mean value was used. During the measurements, the average ambient temperature was 21 °C. The measurement setup according to Fig. 2 (a) yields a self-inductance of 91.83 µH for the inner coil and 99.66 µH for the outer coil. Table I compares the self-inductance results from analytical calculations, simulations, and measurements, showing strong agreement.

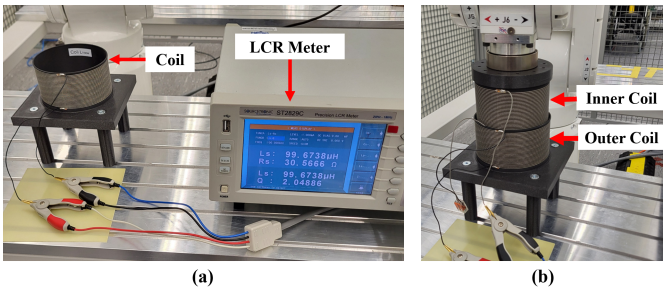

Fig. 2. Setup for measuring the self inductance (a) and series inductance (b)

B. Analysis and Measurement of the Series Inductance

Depending on the degree of overlap between the coils, the series-measured inductance increases or decreases. For the analysis conducted here, the measurement series is divided into ten individual steps over a distance from 0 mm to 50 mm, resulting in a displacement resolution of 5 mm per step.

TABLE I
Self-Inductance of the Coils

Printed Coils	*Analytical* (µH)	*Simulation* (µH)	*Measurement* (µH)
C_O	98.18	99.70	99.66
C_I	89.71	91.09	91.83

In order to enable position detection, the inductance of both coils must be coupled in series. This means that the orientations of both coils are aligned in the same direction, causing the induced fields generated by C_O and C_I to reinforce each other. The previously applied formula (1) is extended to the modified expression (2) to adapt to series inductance L_S.

$$L_S = \frac{\mu_0 \cdot \mu_r \cdot (N_1 + N_2)^2 \cdot \pi \cdot \left(\frac{r_1 + r_2}{2}\right)^2}{(l + \Delta l) + 0.9 \cdot \left(\frac{r_1 + r_2}{2}\right)} \tag{2}$$

In the case of the two coils, it is assumed that the number of turns increases from 30 to 60 due to their series connection. The effective length of the combined coil changes depending on the displacement. For every 5 mm of displacement, 5 mm are added to the initial coil length of 52.5 mm. Due to the different diameters of the inner and outer coils, a mean diameter of 102 mm is assumed. The results of the analytical calculations are presented in Fig. 3.

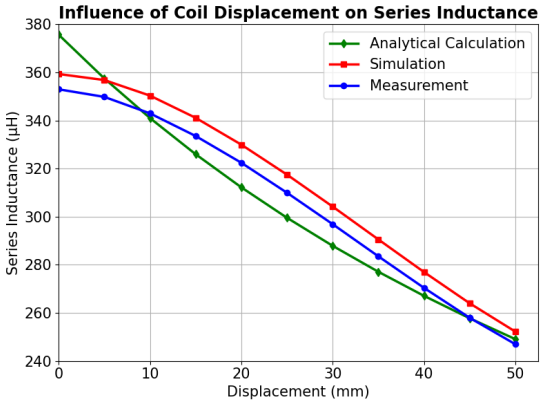

Fig. 3. Comparison of analytical, simulated and measured series inductance under translational displacement

In the simulation, both coils are combined into a single coil aligned in the same turn direction. As shown in Fig. 4, overlapping the coils increases the magnetic flux density inside due to the superposition of their magnetic fields. This increase in magnetic flux density is also reflected in the series inductance values from the simulation, which can be obtained from Fig. 3. The analytical calculation shows that the series inductance decreases with increasing displacement.

The measurement setup in Fig. 2 (b) employs a six-axis robot to enable reproducible and precise displacement for measuring the series inductance at various displacement steps. Similar to the analytical calculation and simulation,

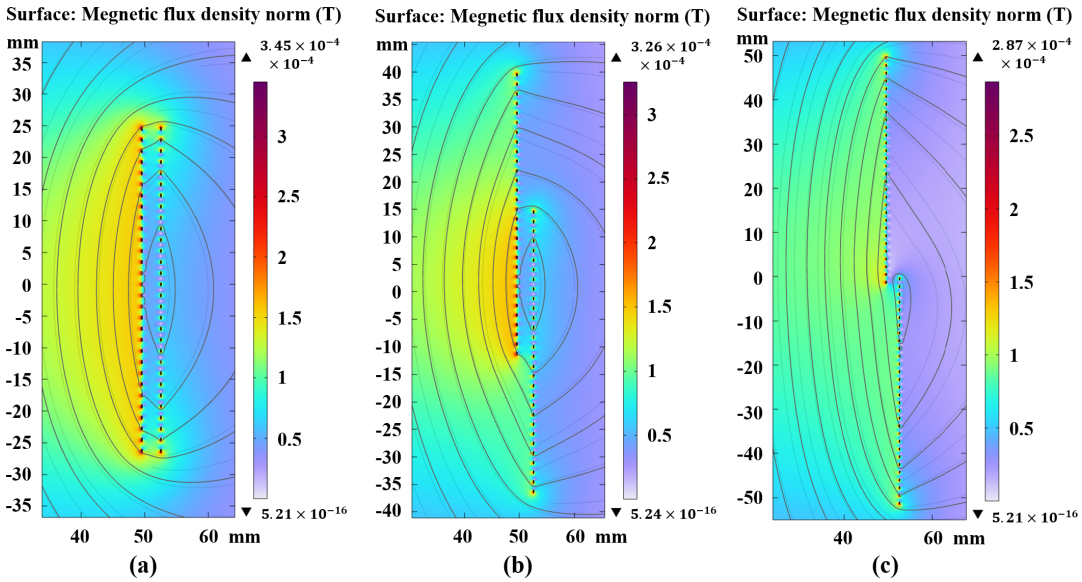

Fig. 4. Magnetic flux density at a displacement of 0 mm (a), 25 mm (b) and 50 mm (c)

the measurement starts at a displacement of 0 mm and is increased in 5 mm steps up to 50 mm. At each measurement point, the series inductance is recorded using the LCR meter, which is connected to both coils as shown in Fig. 5. The upper end of the outer coil is short-circuited with the lower end of the inner coil in order to align the coils in the same winding direction [16].

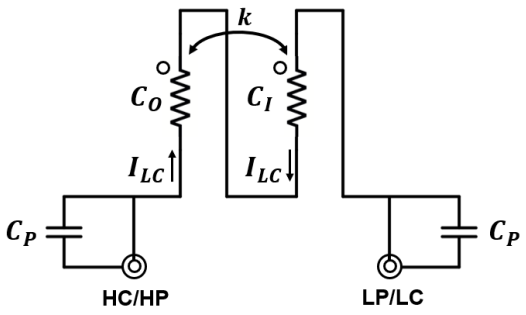

Fig. 5. Connection of the LCR meter in the series coil arrangement with the outer coil C_O and the inner coil C_I - based on [16]

It should be noted that metallic objects, such as the table or the robot flange, in the vicinity of the coils may affect the inductance measurements. The measurements of Fig. 2 were conducted at a height of 90 mm above the table surface to minimize the influence of the table.

The measurement results, as well as the comparison with the analytical calculations and the simulation results, can be obtained in Fig. 3. All values fall within a very narrow range, with the simulation and measurement curves running almost in parallel. The analytical calculation curve shows a different trend compared to the other two. This deviation arises because, in the denominator of (2), 0.9 times the radius is added to the coil length, which reduces the influence of length on the inductance. As a result, the inductance decreases at a slower rate with increasing length. Without this addition, the inductance would be strictly inversely proportional to the length. According to (1), the inductance remains inversely proportional to the length, but in a diminished form.

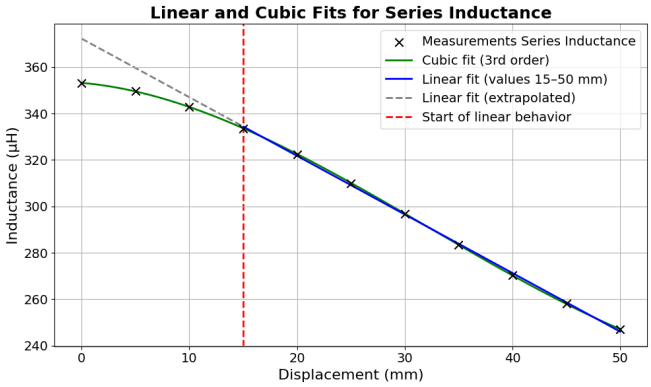

Fig. 6. Linear and cubic fit for the measurements of series inductance

C. Evaluation of the Measurement Results

The results of the measured series inductance are shown in Table II. A detailed examination of Fig. 6 indicates that the measurement results exhibits an approximately linear behavior starting at a displacement of 15 mm and continuing with increasing displacement. The residuals were calculated for a linear and a cubic model to enable a more detailed characterization of the series inductance as a function of displacement. These residuals allow for a direct assessment of the agreement between measurement and model, thereby en-

abling a comparison of the suitability of the two approaches. Table II shows the residuals of the linear and cubic fit.

TABLE II
MEASURED SERIES INDUCTANCE WITH RESIDUALS OF LINEAR AND CUBIC FITS

Displacement (mm)	**Measurement** (µH)	**Linear Residuals** (µH)	**Cubic Residuals** (µH)
0	353.0		-0.21
5	349.8		0.27
10	343.0		0.17
15	333.6	-0.81	-0.06
20	322.4	0.62	-0.18
25	310.0	0.84	-0.14
30	296.9	0.36	-0.01
35	283.5	-0.41	0.07
40	270.4	-0.89	0.14
45	258.0	-0.67	0.04
50	247.0	0.96	-0.09

Residuals are defined as $r_i = y_i - \hat{y}_i$. Linear residuals are valid only in the range 15–50 mm (outside this range the linear model is extrapolation).

The coefficient of determination R^2 is a key metric to assess the quality of fit of the applied model to the measured series inductance data. Based on the acquired data in Table II, the linear fit yields a R^2 of 0.9994 within the displacement range of 15 mm to 50 mm. Considering the entire measurement series from 0 mm to 50 mm, a cubic fit with an R^2 of 0.99998 provides an excellent representation of the curve. As illustrated in Fig. 6, the blue linear regression line provides a close fit to the measured series inductance values in the range from 15 mm to 50 mm, while the extrapolated gray dotted line emphasizes the deviation and the nonlinear behavior observed between 0 mm and 15 mm.

For a more detailed analysis, the residuals of the linear fit are shown in Fig. 7. The linear model provides a reasonable approximation of the measured data between 15 mm and 50 mm, where the residual plot indicates a weak but systematic deviation. The residuals are not randomly distributed around zero but display a slight curvature, suggesting that the relationship is not strictly linear even within this range.

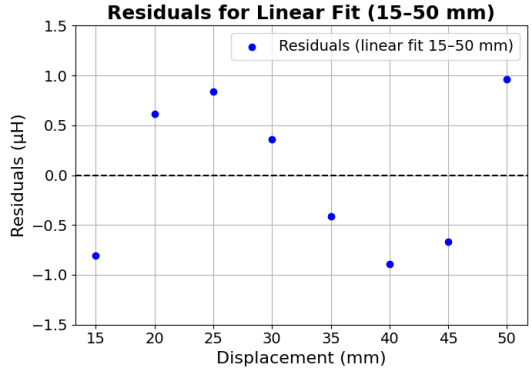

Fig. 7. Residuals of the linear fit for the series inductance from 15 mm to 50 mm

For this reason, a cubic model is applied to a displacement from 0 mm to 50 mm in order to characterize the system behavior for entire measurement series. The green line of the cubic fit in Fig. 6 and the residual plot in Fig. 8 show that the residuals of the third order are significantly smaller than those of the linear model but a subtle pattern remains. The residuals exhibit a weak oscillatory behavior, suggesting that even the cubic model may not fully capture all aspects of the underlying physical process. Nonetheless, given the low magnitude of these residuals, the cubic fit can be considered a very good approximation over the full displacement range, particularly when compared to the clearly inadequate performance of the linear model in the lower displacement region.

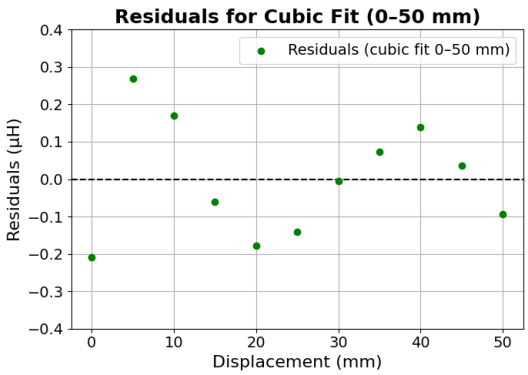

Fig. 8. Residuals of the cubic fit for the series inductance from 0 mm to 50 mm

IV. CONCLUSION

The results demonstrate that displacement sensing can be achieved using two fully additively manufactured coils that move translationally relative to each other. Starting from a displacement of 15 mm, the decrease in series inductance follows an almost linear trend. For the entire displacement range from 0 mm to 50 mm, a cubic third-order fit can be applied. This provides an accurate characterization of the series inductance behavior and allows for reliable interpolation of measurements with a step size smaller than 5 mm. These results highlight the potential for additively manufactured displacement sensors which could be produced in a resource-efficient manner and tailored precisely to the specific application. Further research is expected to address the miniaturization and design optimization of the coils to achieve a finer measurement resolution and enable integration into compact and application-specific systems. Moreover, dynamic measurements are anticipated to investigate the coil behavior under realistic operating conditions on the robot.

ACKNOWLEDGMENT

For grammatical and spelling corrections, ChatGPT by OpenAI and DeepL were partially used in the preparation of this paper, without altering or adding any content.

REFERENCES

[1] M. R. Khosravani and T. Reinicke, "3D-printed sensors: Current progress and future challenges," Sensors and Actuators A: Physical, vol. 305, p. 111916, Apr. 2020, doi: 10.1016/j.sna.2020.111916.

[2] Y. Jiang et al., "Recent Advances in 3D Printed Sensors: Materials, Design, and Manufacturing," Adv Materials Technologies, vol. 8, no. 2, p. 2200492, Jan. 2023, doi: 10.1002/admt.202200492.

[3] L. Stiglmeier, T. M. Wendt, and S. J. Rupitsch, "3-D-Printed Torque Sensors: A Review," IEEE Sensors Journal, vol. 24, no. 12, pp. 18740–18761, Jun. 2024, doi: 10.1109/JSEN.2024.3397919.

[4] S. Schröder, T. M. Wendt, and S. J. Rupitsch, "P29 - Additive Manufactured Capacitive Displacement Sensor Concept, for Adaptive Pin-Array Gripper," in Poster, Nürnberg: AMA Service GmbH, Von-Münchhausen-Str. 49, 31515 Wunstorf, 2024, pp. 536–540. doi: 10.5162/sensoren2024/P29.

[5] N. Hangst, T. M. Wendt, T. Seifert, and S. J. Rupitsch, "Additive Manufactured Sensitive Gripper Jaw for Extended Gripping Force Ranges in Robotics," IEEE Sensors J., vol. 25, no. 16, pp. 30484–30495, Aug. 2025, doi: 10.1109/JSEN.2025.3586583.

[6] L. Stiglmeier, T. M. Wendt, N. Hangst, P. Gawron, and S. J. Rupitsch, "C1.2 - A guideline for the fabrication of fully 3D-printed torque sensor elements - demonstrated based on a real example," Vorträge, Nürnberg: AMA Service GmbH, Von-Münchhausen-Str. 49, 31515 Wunstorf, 2024, pp. 213–220, doi: 10.5162/sensoren2024/C1.2.

[7] A. Benchirouf and O. Kanoun, "Inkjet-Printed Multiwalled Carbon Nanotube Dispersion as Wireless Passive Strain Sensor," Sensors, vol. 24, no. 5, p. 1585, Feb. 2024, doi: 10.3390/s24051585.

[8] F. Corti et al., "Evaluation of Additive Manufacturing for Wireless Power Transfer Applications," IEEE Trans. Ind. Electron., vol. 71, no. 5, pp. 4586–4595, May 2024, doi: 10.1109/TIE.2023.3283679.

[9] T. Hou et al., "Design of 3D Wireless Power Transfer System Based on 3D Printed Electronics," *IEEE Access*, vol. 7, pp. 94793–94805, 2019, doi: 10.1109/ACCESS.2019.2928948.

[10] M. G. Kisić, K. B. Babković, and M. S. Damnjanović, "Wireless Inductive Displacement Sensor 3-D Printed Using Additive Technology," IEEE Trans. Magn., vol. 59, no. 11, pp. 1–6, Nov. 2023, doi: 10.1109/TMAG.2023.3293962.

[11] G. Han, Y. Liu, S. Guo, T. Han, and Q. Li, "Design of coaxial coupled structure for distance-insensitive wireless power transfer," Rev. Sci. Instrum., vol. 90, no. 7, p. 074708, Jul. 2019, doi: 10.1063/1.5095210.

[12] X. Zhang, H. Meng, B. Wei, S. Wang, and Q. Yang, "Mutual inductance calculation for coils with misalignment in wireless power transfer," J. Eng., vol. 2019, no. 16, pp. 1041–1044, Mar. 2019, doi: 10.1049/joe.2018.8670.

[13] B. Kallel, O. Kanoun, and H. Trabelsi, "Large air gap misalignment tolerable multi-coil inductive power transfer for wireless sensors," IET Power Electronics, vol. 9, no. 8, pp. 1768–1774, Jun. 2016, doi: 10.1049/iet-pel.2015.0800.

[14] R. Waltersbacher, L. Stiglmeier, and T. M. Wendt, "Additive Manufacturing for Inductive Power Transfer in Robotic Applications," in 2025 The 16th International Conference on Mechanical and Intelligent Manufacturing Technologies (ICMIMT), Cape Town, South Africa: IEEE, May 2025, pp. 143–150. doi: 10.1109/ICMIMT65123.2025.11092047.

[15] G. Welytschko, "Die Berechnung der Selbstinduktion von einlagigen Zylinderspulen," Arch. Für Elektrotechnik, vol. 37, no. 11, pp. 520–533, Nov. 1943, doi: 10.1007/BF02094794.

[16] A. Celentano et al., "Mutual Inductance Measurement in Wireless Power Transfer Systems Operating in the MHz Range," IEEE Trans. Circuits Syst. II, vol. 71, no. 3, pp. 1715–1720, Mar. 2024, doi: 10.1109/TCSII.2023.3334432.